Effect of the charge-density-wave gap on the Raman spectra in orthorhombic TaS_3

S. Sugai
Department of Physics, Faculty of Science, Osaka University, 1-1 Machikane-yama, Toyonaka, Osaka 560, Japan
(Received 4 May 1983)

Lattice vibrations in orthorhombic TaS_3 have been investigated by polarized Raman scattering above and below the charge-density-wave (CDW) phase-transition temperature of 218 K. Below T_c, satellite peaks become clear on the lower-energy slopes of the dominant peaks and increase the intensity with decreasing temperature. The main peaks at room temperature decrease the intensity and shift to the higher-energy side below T_c. This one-dimensional material consists of 24 trigonal prismatic chains in the unit cell. Each chain which has different tendency for the CDW formation is assumed to give one of the satellite peaks. In the chains with large CDW amplitude, the decrease in the number of free carriers due to the formation of the CDW gap at the Fermi level leads to a decrease in the scattering intensity from the intraband process as well as an increase in the phonon energy. The temperature dependence of the scattering intensity is compared with the calculated intraband scattering intensity, which is proportional to the bare electronic susceptibility of the electron gas in the conduction band with the CDW gap.

I. INTRODUCTION

Transition-metal trichalcogenides which consist of a parallel arrangement of trigonal prismatic chains are known as a group of typical one-dimensional materials. The variety of the arrangements of chains in the unit cell makes different types of crystal structure and physical property.[1,2] Three compounds, TaS_3, $TaSe_3$, and $NbSe_3$, are metallic at high temperatures, while other sulfides and selenides of Ti, Zr, Hf, and Nb are semiconducting. Two metallic compounds, TaS_3 and $NbSe_3$, exhibit charge-density-wave (CDW) phase transition at low temperatures,[3,4] which is characteristic phase transition in low-dimensional materials. A superconducting phase transition is known in $TaSe_3$ and $NbSe_3$ at low temperatures and with pressure.[5,6]

The CDW phase transition in TaS_3 was first reported by Sambongi *et al.*[5] Electron and x-ray diffraction experiments have been done to observe the crystal structure,[3,4,7–9] but the atomic positions in orthorhombic TaS_3 are not known yet. The lattice vibrations were investigated by Tsang *et al.*[10] Transport experiments have also been performed to investigate the electric properties.[3,11–17] The non-Ohmic conductivity and the specific noise of current, which are usually attributed to the collective sliding motion of the CDW, have been observed in TaS_3 (Ref. 18) as well as $NbSe_3$.[19]

Recently, the existence of two different types of crystal structure has been reported in the normal phase of TaS_3. One type is an orthorhombic structure[20] and the other is a monoclinic structure.[21] Both types show CDW phase transitions at different temperatures. Sometimes both structures coexist in one crystal-growing ampoule. Though the space group of the orthorhombic structure had been reported to be $C222_1$, a very recent experiment by the convergent-beam electron-diffraction method revealed the microdomain structure and observed the $Pmn2_1$ (C_{2v}^7) symmetry in the domain at room temperature.[22] The dimensions of the unit cell are $a=36.804$ Å, $b=15.177$ Å, and $c=3.340$ Å (chain direction), including 24 chains. The orthorhombic TaS_3 has one transition temperature (T_c) at 218 K determined from the maximum of the temperature derivative of the conductivity $|d\ln\sigma_c/dT|$. Even in the normal phase x-ray diffraction shows diffuse scattering lines at $Q_c=0.25c^*$ due to the finite amplitude of the CDW along the c axis by the phase fluctuation among the chains.[3] Below T_c satellite spots are observed at $0.5a^*+0.125b^*+0.25c^*$ (Ref. 9) due to the formation of the superlattice of $2a\times 8b\times 4c$. The electric conductivity measurement shows semiconducting behavior below T_c. The monoclinic TaS_3 had been reported to belong to the $P2_1/m$ (C_{2h}^2) space group,[21] but recent convergent-beam electron-diffraction measurements showed $B2/m$ (C_{2h}^3) symmetry.[22] The unit-cell dimensions are $a=9.515$, $b=3.3412$ (chain direction), and $c=14.912$ Å, and $\beta=109.99°$. The monoclinic TaS_3 has two transition points at 240 and 160 K. The lowest-temperature phase is a semiconducting state.

The formation of the CDW is essentially accompanied by the lattice displacement. Tsang *et al.*[10] reported the lattice vibrations of TaS_3 measured by Raman scattering, with their emphasis on the anomaly of the Raman linewidth of specific phonon peaks. The anomaly was observed in the phonon peaks of 283, 405, and 496 cm^{-1} at 200, 150, and 60 K, respectively. They analyzed the anomaly by the electron-phonon interaction related to the electronic excitation through the CDW-created gap, and estimated the temperature dependence of the energy gap in the CDW state. But our experimental results by high-resolution polarized Raman scattering with the use of a single crystal are different from their results.

This experiment revealed the splitting of the 284-cm^{-1} line below T_c, instead of the increase of the linewidth. The anomalies in the 405- and 496-cm^{-1} lines were not noticed at the temperatures at which Tsang *et al.* observed anomalous behavior in the linewidth. At room temperature about ten lines with relatively large intensities are observed in the energy range from 50 to 500 cm^{-1}. Some of

them are broad and asymmetric due to the broad satellite peaks close to the lower-energy side of the main peaks. The satellite peaks become strong and clearly resolved with decreasing temperature through T_c. The relative intensities of the main peaks at high temperatures decrease with cooling below T_c.

The unit cell of orthorhombic TaS_3 is assumed to contain several types of triangular chains with slightly different cross sections, deducing from the case of monoclinic TaS_3 (Ref. 21) and other transition-metal trichalcogenides.[2,21] Each chain contributes to give one of the satellite peaks, if the interchain interaction is small. Shima calculated the band structure of $NbSe_3$ and showed that each chain has the corresponding Fermi surfaces, which have its own nesting condition that is related to the different phase-transition temperature.[23,24] A similar situation is expected to be satisfied in TaS_3. Each chain has a different amplitude of the CDW and the energy gap below T_c because the nesting of the Fermi surfaces is sensitive to the shape of the chain. In the chain with large CDW amplitude, the generated large CDW energy gap reduces the number of free carriers and decreases the screening of the atomic potential, so that the phonon energy increases. At the same time the formation of the CDW gap reduces the Raman cross section of the intraband term (diamagnetic term),[25,26] because this term contributes only in metal and the cross section is proportional to the density of states at the Fermi level. The temperature dependence of the scattering intensity is compared with the calculated intraband scattering intensity in a one-dimensional conduction band with the CDW gap.

Our experimental results are presented in Sec. II. The mode assignment and the discussion about the Raman scattering intensity in the CDW state are given in Sec. III. The intraband Raman process in metal is presented in the Appendix.

II. EXPERIMENTAL RESULTS

Single crystals of orthorhombic TaS_3 were grown by a vapor-transport method. The typical sizes were 15μm (in the a-axis direction)$\times$40μm (along b)$\times$5μm (along c). One single crystal was set in a variable temperature cryostat where cold helium gas flows on the sample surface. The experiment was made in a backscattering configuration with a 70-mW argon-ion laser at 5145 Å. The incident beam is in the (011) plane with an incident angle of about 30°. A cylindrical lens was used to illuminate the sample, effectively preventing temperature rise. The weak scattering probability required about 10 h for 500 cm^{-1} scanning. The details of the experimental system are described elsewhere.[27]

The observed Raman spectra of the $a(b,b)\bar{a}$ polarization configuration are shown in Fig. 1. The notation $a(b,b)\bar{a}$ means the propagation and polarization directions of the incident light, and the polarization and propagation directions of the scattered light, from left to right in order. In this polarization configuration the element b of the Raman tensor for the A_1 mode participates in the scattering.[28] The normalized scattering intensity is obtained from dividing the observed intensity by the statistical factor $(n+1)$ for the Stokes side, where n is the Bose distribution function. The dominant peaks are 284, 336, 374, 404, and 498 cm^{-1} at room temperature. With decreasing temperature, the broad asymmetric peaks of 284, 336, 404, and 498 cm^{-1} separate into many lines due to the narrowing and the increasing of the scattering intensity of the satellite peaks.

The normal modes of each chain are expected to be responsible for the main structure of the Raman spectra in TaS_3, because the interchain interaction is small as observed in the large anisotropy of the conductivity, $\sigma_c/\sigma_b \simeq 150$.[29] Two mechanisms are considered for the origin of the satellite peaks. The first is that the small difference in the normal-mode energy between the chains with slightly different dimensions in the unit cell gives satellite peaks. The second is that the modulation of the chains in the CDW phase gives the satellite peaks. At room temperature many peaks have the traces of the satellite peaks as asymmetric line shapes or shoulders. Above T_c there is no CDW in the mean-field approximation, but the thermodynamic fluctuation gives the local CDW even above the T_c. Such fluctuation causes the split of the phonon energy even in the normal phase. Above the T_c the energy splitting between the main peak and the satellite peak, which is noticed to be a shoulder, is almost constant in the 284- and 498-cm^{-1} modes. If the satellite peaks at room temperature come from the fluctuation, large temperature dependence is expected differently from the experimental results. We assign therefore the origin of the main and the satellite peaks to the same normal modes of the different chains with slightly different dimensions. The satellite peaks which become clear at low temperatures are grouped by the energy of the main peaks at room temperature as indicated at the lower part of the 19-K spectrum of Fig. 1. The detailed discussions are given in Sec. III.

The total scattering intensity increases suddenly below T_c in this polarization configuration as shown in Fig. 2. The sudden increase below T_c is also observed in the $a(b,c)\bar{a}$ polarization configuration. The Raman spectra in the $a(c,c)\bar{a}$ and the $a(c,b)\bar{a}$ configurations do not show a sudden increase. This increase in the scattering intensity is probably attributed to the change in the electronic band structure responsible for the dipole transition parallel to the b axis. The phase correlation between the chains below T_c may contribute to this sudden change. The large temperature derivative of the electric resistivity at T_c may be related to this change of the electronic states.

Figure 3 shows the temperature dependence of the phonon energies. The temperature dependence is small except for the 284-cm^{-1} peak. Above 200 K the peak designated as $\times$ in Fig. 1 approaches the 284-cm^{-1} peak. The details of these peak energies are shown in Fig. 4. The bars indicate the full linewidths at half-maximum. The peak positions and the linewidths are obtained from a computer fitting by the superposition of Gaussian lines taking into account the apparatus resolution determined by the spectrometer. The splitting of the line designated $\times$ from the

higher-energy mode is clearly seen below 200 K. Figure 5 shows the temperature dependence of the full linewidth at half-maximum. The peaks of 284 and 498 cm^{-1} are very asymmetric and have lower-energy tails at high temperatures because small peaks which are resolved at low temperatures are superimposed on the lower-energy sides. The peaks of 160, 336, and 404 cm^{-1} are narrow even at high temperatures. The minimum linewidth of the experi-

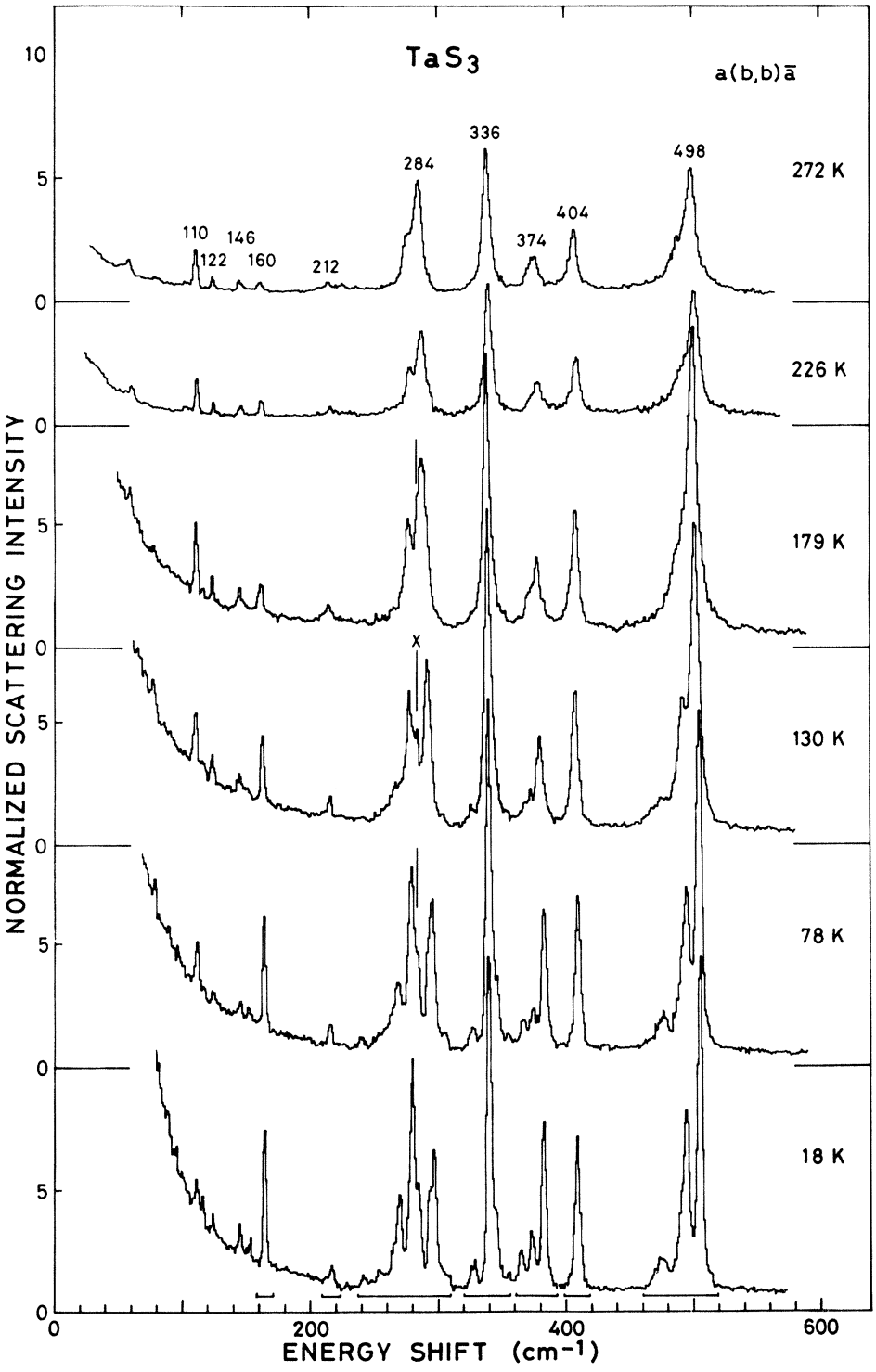

FIG. 1. Raman spectra of TaS_3 in the $a(b,b)\bar{a}$ polarization configuration. Below T_c, 218 K, many satellite peaks become clear on the lower-energy sides of the main peaks. They are grouped as shown below in the 18-K spectra. Peak designated $\times$ diverges from the 284-cm^{-1} main peak below the T_c.

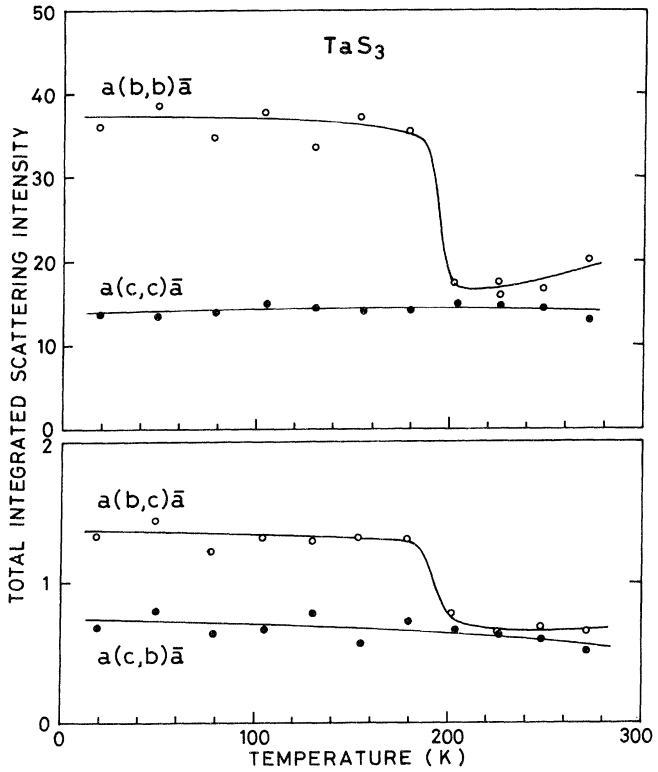

FIG. 2. Temperature dependence of the total integrated scattering intensity of whole peaks for each polarization configuration.

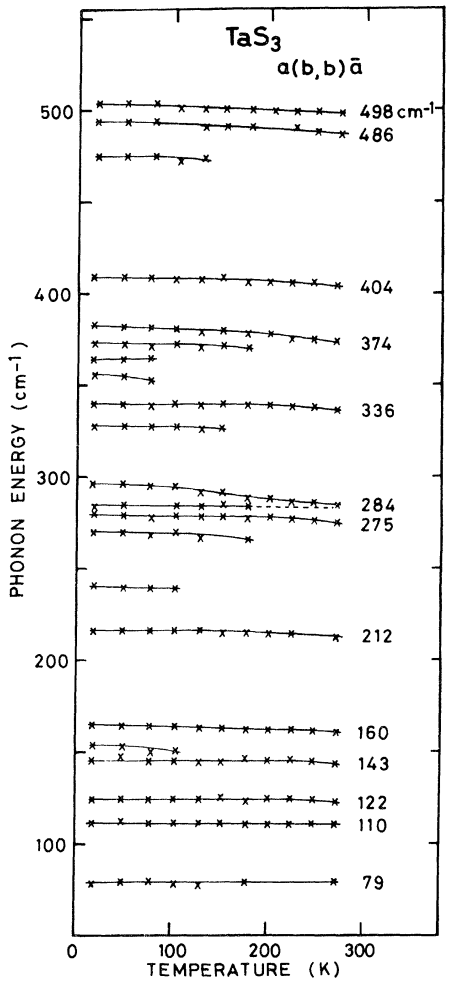

FIG. 3. Temperature dependence of the phonon energies in the $a(b,b)\bar{a}$ polarization configuration.

mental system is 2.5 cm^{-1}. Figure 6 shows the relative integrated scattering intensity of each group shown in Fig. 1 in the unit of the total integrated scattering intensity of whole peaks. The scattering intensity of the 160-cm^{-1} peak strongly increases at low temperatures compared with other peaks. Figure 7 shows the relative integrated scattering intensity between the main peak and the satellite peaks in each group. Each peak is named by the energy at 18 K. At high temperatures the intensity of each component is obtained by assuming a symmetric line shape. With decreasing temperature the relative intensity starts to change at about 200 K and becomes constant at about 100 K. The relative intensity of the higher-energy peak in each group is always strong at high temperatures.

Figure 8 shows the Raman spectra in the $a(c,c)\bar{a}$ polarization configuration. The Raman tensor element c of the A_1 mode is responsible in this configuration.[28] The remark is due to the absence of the 110- and 336-cm^{-1} peaks which are strong in the $a(b,b)\bar{a}$ configuration, in spite of the observation of the same A_1 modes in both polarization configurations. The peak of 285 cm^{-1} is relatively stronger than other peaks. Figure 9 shows the temperature dependence of the peak energies. Above 200 K the 285-cm^{-1} peak joins with the almost temperature-independent peak, as in the case of the $a(b,b)\bar{a}$ configuration. The linewidths are shown in Fig. 10. The relative integrated scattering intensities are shown in Fig. 11 in the unit of the total scattering intensity of whole peaks. The

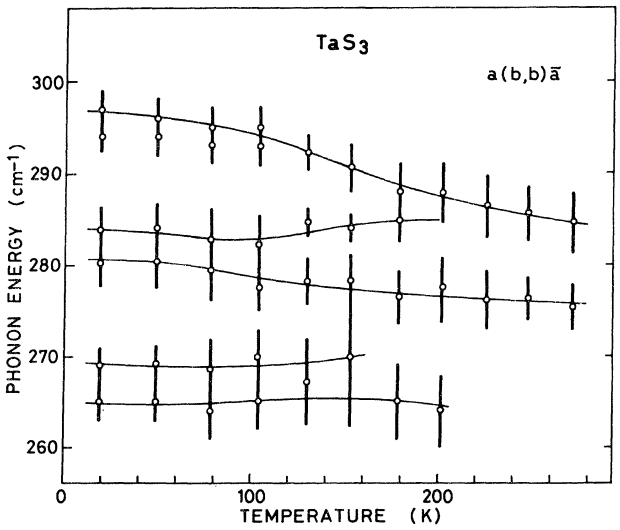

FIG. 4. Temperature dependence of the energies and the linewidths of the main and satellite peaks in the 284-cm^{-1} group. Bars indicate the full linewidth at half-maximum.

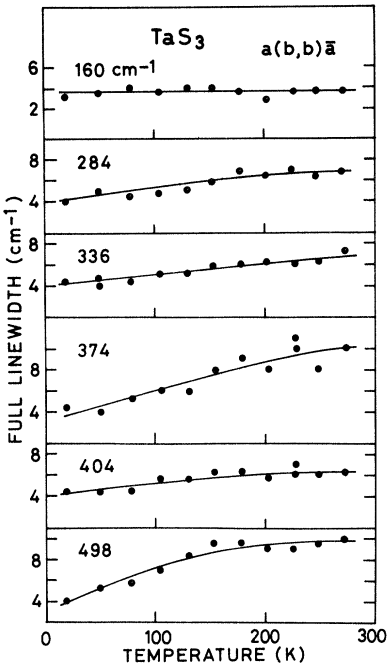

FIG. 5. Full linewidths of the dominant peaks as a function of temperature in the $a(b,b)\bar{a}$ polarization configuration.

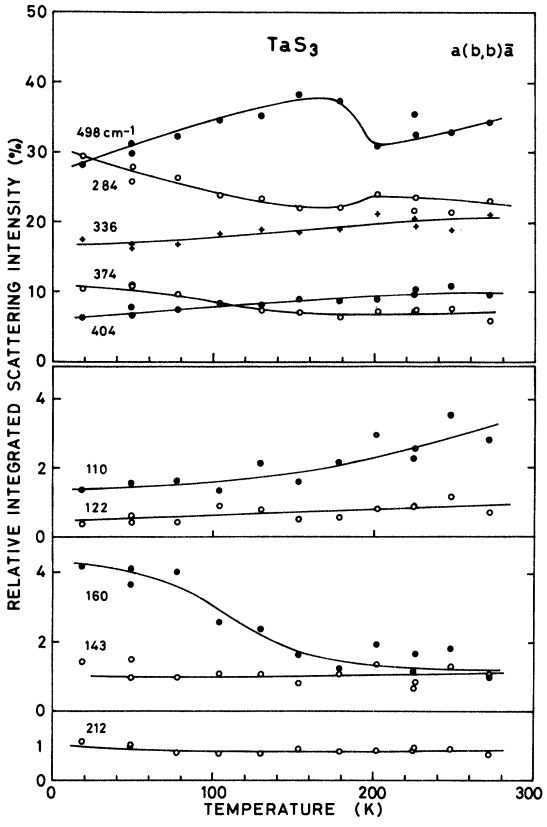

FIG. 6. Temperature dependence of the relative integrated scattering intensity of each group in the unit of the total scattering intensity of whole peaks in the $a(b,b)\bar{a}$ polarization configuration.

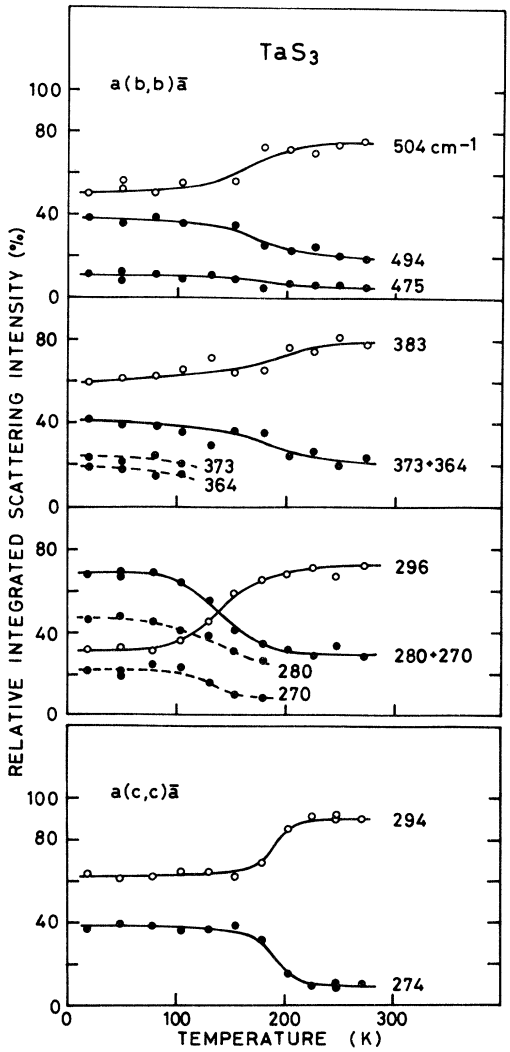

FIG. 7. Temperature dependence of the relative integrated scattering intensity within each group.

peak at 160 cm^{-1} is narrow even at high temperatures and the intensity decreases with cooling as opposed to the case of the $a(b,b)\bar{a}$ configuration. The temperature dependence of the relative integrated scattering intensity between the main peak and the satellite peaks of the 285-cm^{-1} group is shown in Fig. 7. The change in the relative intensity of the main peak is more rapid and it occurs at a higher temperature compared with the $a(b,b)\bar{a}$ configuration.

Figure 12 shows the Raman spectra of the $a(c,b)\bar{a}$ polarization configuration. In this configuration the B_2 modes are active. Almost the same spectra are obtained in the $a(b,c)\bar{a}$ configuration. The scattering intensity in this polarization is weak compared with the $a(b,b)\bar{a}$ and $a(c,c)\bar{a}$ configurations.

III. DISCUSSION

A. Mode assignment

A large number of atoms, as many as 96, are included in the unit cell and the atomic positions are not known

even in the normal phase. Below T_c the unit-cell volume increases by 64 times than that of the normal phase. The observed peaks are much less in number than the expected peaks. This means that many modes have almost degenerate energy. If 24 chains in the unit cell have almost the same dimensions to each other and the interchain interaction is small, the normal mode in each chain has almost the same energy. A bundle of the normal modes in the 24

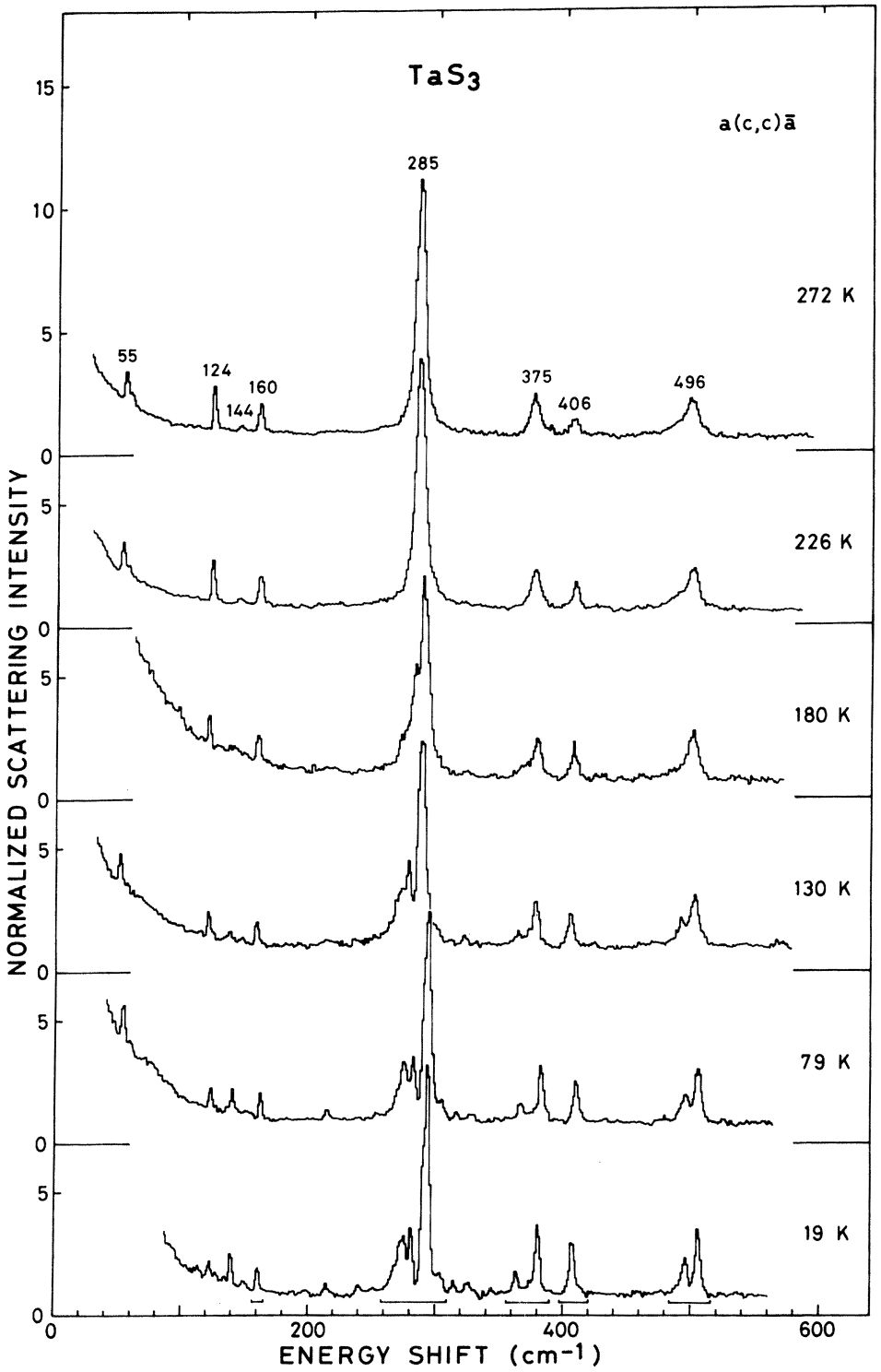

FIG. 8. Raman spectra in the $a(c,c)\bar{a}$ polarization configuration. Absence of the dominant peaks at 110 and 336 cm^{-1} in the $a(b,b)\bar{a}$ configuration should be noted.

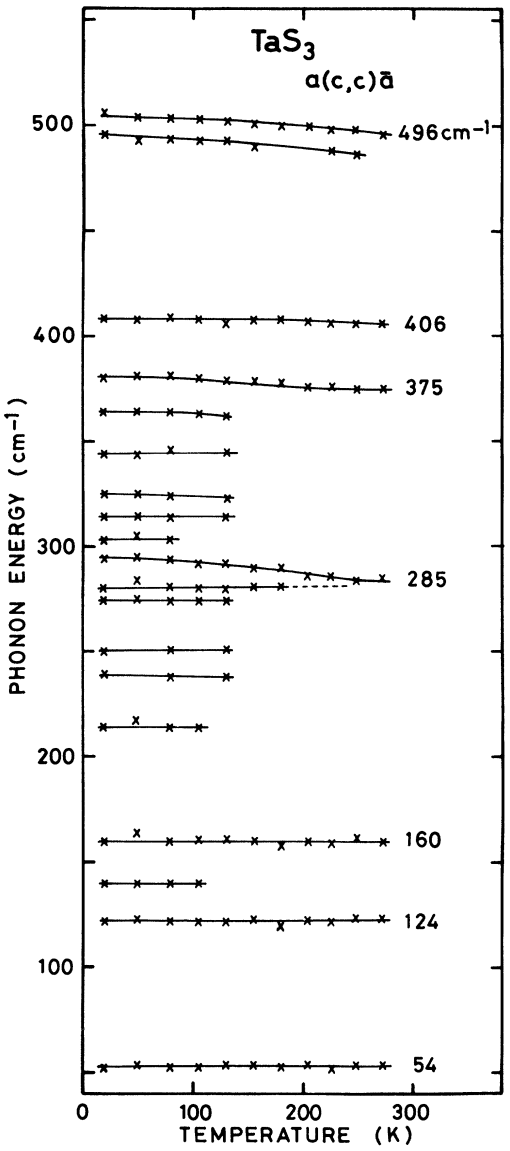

FIG. 9. Temperature dependence of the peak energies in the $a(c,c)\bar{a}$ polarization configuration.

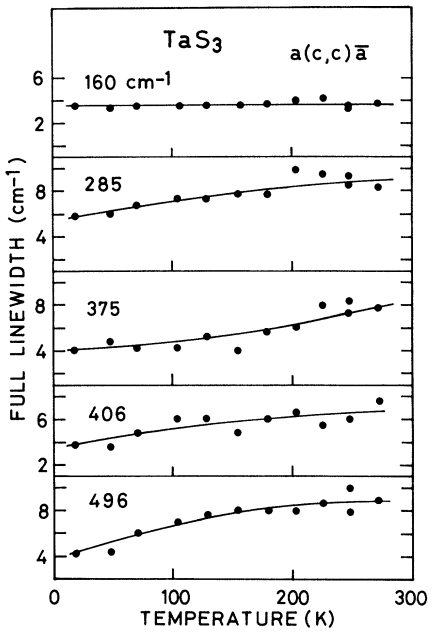

FIG. 10. Temperature dependence of the full linewidths of the dominant peaks in the $a(c,c)\bar{a}$ polarization configuration.

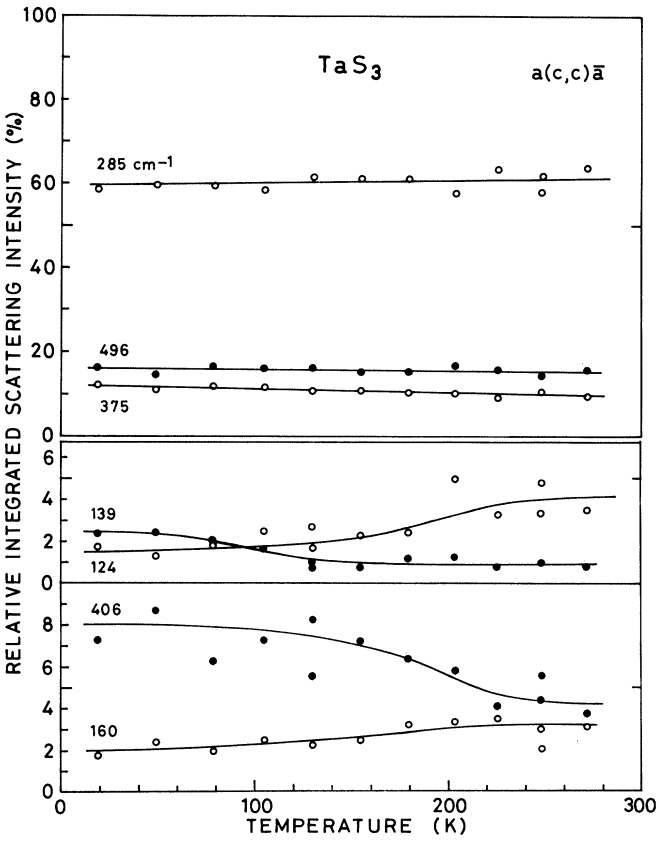

FIG. 11. Temperature dependence of the relative integrated scattering intensity of each group in the unit of the total scattering intensity of the whole peaks in the $a(c,c)\bar{a}$ polarization configuration.

chains makes a broad line in the Raman spectra. The interchain interaction is expected to be weak in TaS_3 from the large conductivity anisotropy, $\sigma_c/\sigma_b \simeq 150$ and $\sigma_c/\sigma_a \simeq 750$.[29] The structure of the chains in the orthorhombic TaS_3 is inferred from the monoclinic TaS_3 structure observed by x-ray diffraction.[21]

The unit cell of the monoclinic TaS_3 has six chains. Three of them are independent because the crystal structure has inversion symmetry. The dimensions of the triangular cross sections of the three chains are $2.068\times3.588\times3.530$, $2.105\times3.605\times3.541$, and $2.835\times3.392\times3.389$ Å.[21] These cross sections can be approximated by two types of isosceles triangles. Many chains in the orthorhombic TaS_3 are expected to have the size of the cross section close to $2.068\times3.588\times3.530$ Å because the observed phonon energy of 498 cm^{-1} is very

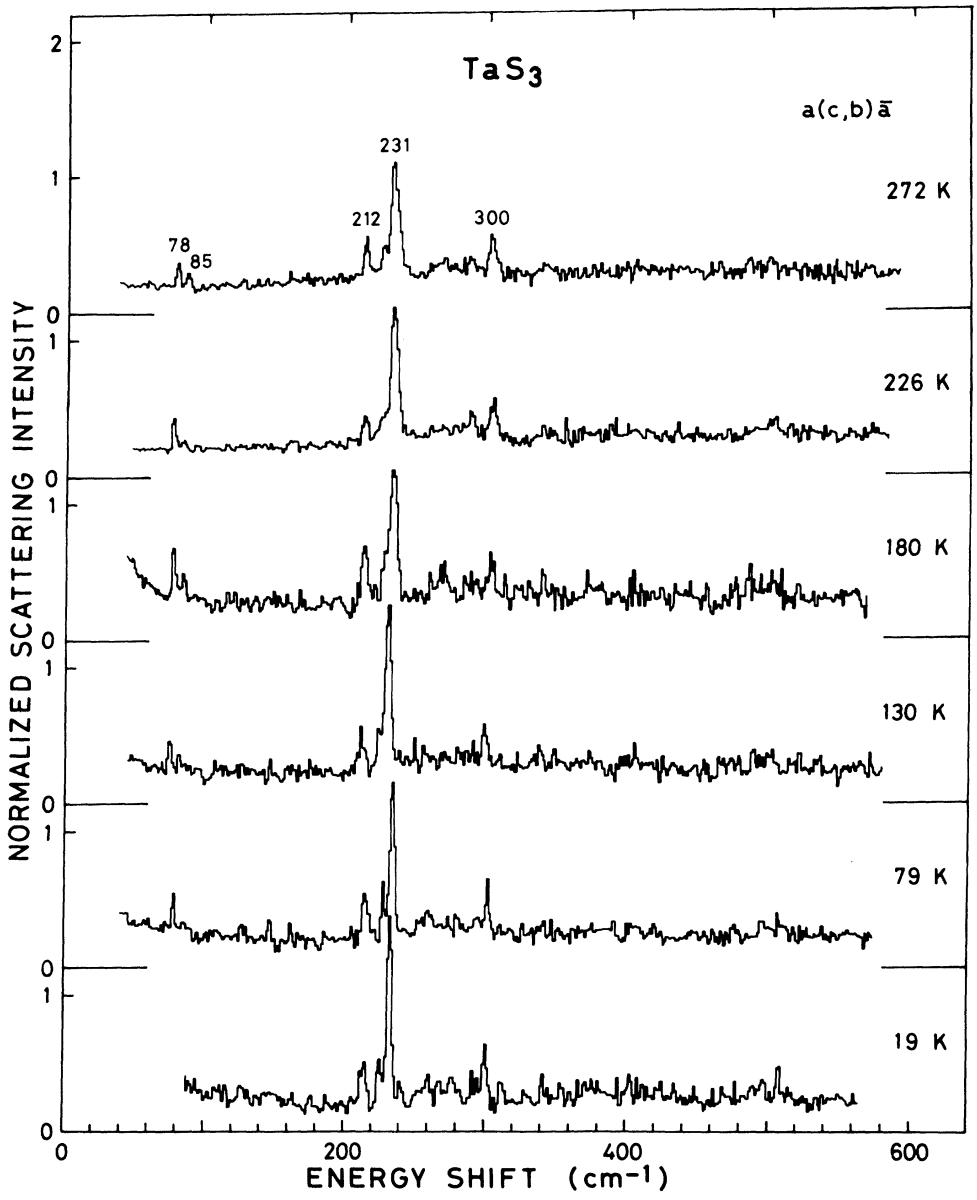

FIG. 12. Raman spectra in the $a(c,b)\bar{a}$ polarization configuration.

close to the energy of the S—S bond-stretching mode in the materials with the interatomic distance of 2.05 Å. The symmetry of the unit cell of the isosceles-triangular prismatic chain is orthorhombic C_{2v} with the twofold axis perpendicular to the chain axis. The normal modes of lattice vibrations in the chain are $4A_1+A_2+4B_1+3B_2$. Each one of A_1, B_1, and B_2 modes is the acoustic mode. Nine normal modes of optical phonons are shown in Fig. 13. The Raman tensors $A_1(y)$, A_2, $B_1(x)$, and $B_2(z)$ are, respectively,

$$\begin{bmatrix} a & 0 & 0 \\ 0 & b & 0 \\ 0 & 0 & c \end{bmatrix}, \quad \begin{bmatrix} 0 & 0 & d \\ 0 & 0 & 0 \\ d & 0 & 0 \end{bmatrix}, \quad \begin{bmatrix} 0 & e & 0 \\ e & 0 & 0 \\ 0 & 0 & 0 \end{bmatrix}, \quad \begin{bmatrix} 0 & 0 & 0 \\ 0 & 0 & f \\ 0 & f & 0 \end{bmatrix}$$

for the coordinate axes shown in Fig. 13. The b and c axes of the orthorhombic TaS_3 structure are in the x-y plane of Fig. 13. The A_1 and B_1 modes are active in the $a(b,b)\bar{a}$ polarization configuration, the A_1 mode in the $a(c,c)\bar{a}$, and the A_2 and B_2 modes in the $a(b,c)\bar{a}$. The highest-energy peak of 498 cm^{-1} in TaS_3 is assigned to the A_1 (ν_3) mode. The S-S interatomic distance of the S_8 ring in orthorhombic sulfur is 2.048 Å (Ref. 30), which is very close to the shortest S-S distance of the isosceles-triangular prism. The phonon energy of 498 cm^{-1} is close to the energy of the A_1 symmetric mode of the S_8 ring, 470 cm^{-1} in a crystal and 475 cm^{-1} in liquid.[30] The energy of the 284-cm^{-1} mode is very close to the 286-cm^{-1} E_{2g} mode in 2H-TaS_2.[31] In this mode the Ta atoms and S atoms move to the counter direction in the x-y plane. The

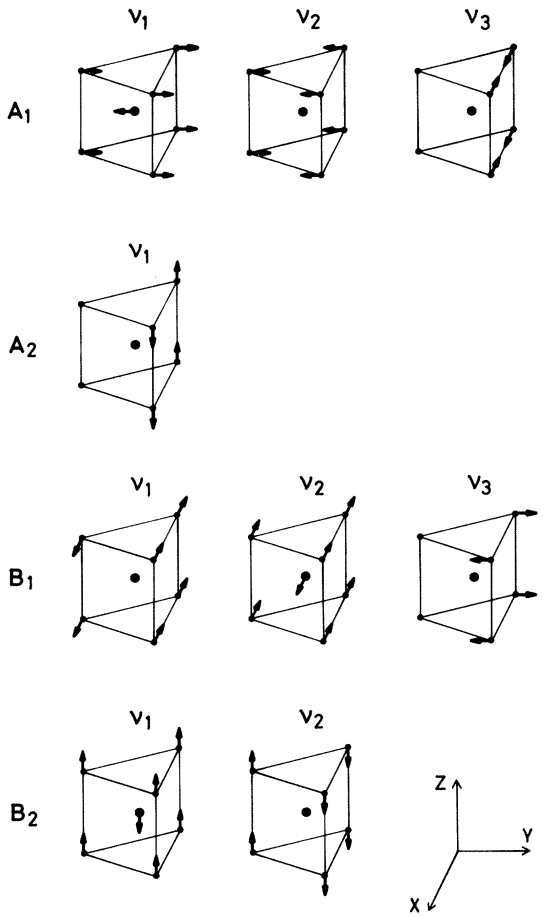

FIG. 13. Normal modes of the unit cell of the isosceles-triangular prismatic chain which is the idealized constitutional element of the orthorhombic TaS_3. Note that the choice of the coordinate axes is different from the normal denomination.

atomic movement of this mode is assigned to the A_1 (ν_1) mode and the B_1 (ν_2) mode. The large change in the 284-cm^{-1} peak on temperature is related to the atomic motion of Ta in this mode because the d-electron band of Ta causes the CDW. The peak at 374 cm^{-1} is tentatively assigned to the A_1 (ν_2) mode. The peaks of 110 and 336 cm^{-1} are observed only in the $a(b,b)\bar{a}$ spectra. Therefore, the 110-cm^{-1} mode is assigned to the B_1 (ν_1) mode and the 336-cm^{-1} mode to the B_1 (ν_3) mode. The 285-cm^{-1} peak in the $a(c,c)\bar{a}$ configuration is assigned to the A_1 (ν_1) mode. The 231-cm^{-1} peak in the $a(c,b)\bar{a}$ polarization spectra has a satellite peak at low temperatures. This mode is tentatively assigned to the B_2 (ν_1) mode. The modes realized by diagonalizing the secular equation of atomic motion are a linear combination of the normal modes with the same symmetry. The modes with satellite peaks at low temperatures are expected to be related to the Ta atomic motion.

In this commensurate CDW phase the dimensions of the unit cell increases to $2a\times 8b\times 4c$, and 64 times as many as the modes in the normal phase are expected in the Raman spectra due to the folding of the phonon modes at the large-wave-vector points to the Γ point. The peaks from the folding of the wave-vector points in the a-b plane is expected to locate in the vicinity of the original Γ-point mode because the dispersion in the direction perpendicular to the chain axis is expected to be small due to the good one dimensionality. The new peaks folded from the $0.25c^*$, $0.5c^*$, and $0.75c^*$ appear probably in the different energy regions from the original Γ-point modes because the dispersion along the c direction is not small, and also the Kohn-anomaly effect modifies the dispersion strongly. Only one part of the modes folded from the large-wave-vector points is related to the Kohn-anomaly modes, and the others are folded from non-Kohn-anomaly modes due to the formation of the superlattice. The CDW modes related to the Kohn anomaly are expected to appear in the low-energy region similar to two-dimensional transition-metal dichalcogenides[27] if the phase transition is close to the second order. But the strong light elastically scattered from the sample surface prevented the observation of low-energy soft CDW modes.

At low temperatures satellite peaks appear in the modes at 284, 336, 374, and 498 cm^{-1} in the $a(b,b)\bar{a}$ spectra, and 285, 375, and 496 cm^{-1} in the $a(c,c)\bar{a}$ spectra. One satellite peak which diverges from the main peak below T_c is observed in the 284-cm^{-1} group. Many satellite peaks do not appear by the divergence from the original peak at T_c, but by the increase in the intensity keeping the energy constant. The temperature dependence of the intensity of the satellite peaks has the same tendency in all groups. The relative intensity of the lower-energy peak in each group increases with decreasing temperature.

It is known that in the materials with the CDW phase transition the interband Raman scattering intensity due to the phonons related to the Kohn-anomaly modes is strongly enhanced by the large generalized electronic susceptibility at the wave vector of $2k_F$, $g^2\chi(2k_F)$, below T_c.[27,32] Here g is the electron—Kohn-anomaly-phonon interaction parameter. It is assumed that each chain in the unit cell has a different tendency for the formation of the CDW, and the modes in the chains which cause the CDW transition have large Raman intensity. Such chains create a large energy gap below T_c. The decrease in the free carriers reduces the screening of the atomic potential so that the phonon energy increases. The decrease in the density of states at the Fermi energy decreases the Raman cross section of the intraband process as written in the following. With decreasing temperature below T_c, the chains which do not have enough nesting condition of the Fermi surfaces continue still to increase the generalized susceptibility and enhance the scattering intensity.

B. Intraband Raman process and the CDW gap

For Raman scattering in metal the intraband process contributes to the scattering probability[25,26] as well as the interband process,[28] which is the only important mechanism in insulating materials. In the intraband process an electron in the partially filled conduction band is excited to the same band by the interaction with photons through the A^2 term, where A is the vector potential of the incident

and scattered photons. This process contributes to the scattering by the totally symmetric phonons in the parallel polarization configuration of the incident and scattered lights. The details are discussed in the Appendix. The scattering probability of this process is very sensitive to the density of states at the Fermi level. The formation of the CDW gap at the Fermi surface reduces the scattering probability from this process. The differential cross section from this process is proportional to the square of the bare electronic susceptibility $\chi_0(q,\omega_0)$ of the conduction band,[25] where

$$\chi_0(q,\omega_0)=\sum_k \frac{f(\epsilon^c_{k-q})-f(\epsilon^c_k)}{\epsilon^c_{k-q}-\epsilon^c_k-\omega_0-i\delta} . \tag{1}$$

Here q is close to zero from the momentum conservation with the incident and the scattered lights. The susceptibility at $q\simeq 0$ in the intraband process gives a different temperature dependence from the susceptibility at $q\simeq 2k_F$, which is the characteristic quantity for the CDW phase transition and gives the strong two-phonon Raman peaks in $2H$ compounds.[27,32]

For the long coherence limit the energy gap 2Δ of the CDW state is expressed by the same form with the superconducting gap

$$1=\frac{|g_{2k_F}|^2\rho_0(E_F)}{\omega_{2k_F}\Omega} \times\int_0^{E_B}\frac{\tanh[(E_k^2+\Delta^2)^{1/2}/(2k_BT)]}{(E_k^2+\Delta^2)^{1/2}}dE_k , \tag{2}$$

where ρ is the density of states, g is the electron-phonon interaction parameter, ω_0 is the phonon energy, and Ω is the volume of the system. McMillan[33] showed that in the case of two-dimensional material $2H$-$TaSe_2$, the long-coherence model, is not applicable. In the short-coherence limit the phonon entropy is very important and the fluctuation of the order parameter is very large even above T_c. In this case the energy gap at 0 K is of the order of $7k_BT_c$ or greater, which is larger than the gap of $3.52k_BT_c$ in the long-coherence limit. In TaS_3 the energy gap estimated from the activation energy of the electric resistivity is about 1200 K,[11] which is 1.56 times larger than the gap energy 767 K obtained from Eq. (2).

Figures 14(a) and 14(b) show the bare susceptibility $\chi_0(q,\omega_0)$ for the phonon energy $\omega_0=284$ (409 K) and 504 cm^{-1} (725 K) as a function of temperature with the parameters of the k_Fq/m $(=\epsilon_{k_F-q}-\epsilon_{k_F})$ and the gap energy at 0 K. The gap energy in the CDW state is assumed to be the superconducting gap given by Eq. (2), curve A in Fig. 14(c), and 1.56 times the superconducting gap, curve B. The electronic susceptibility as a function of the gap energy is sensitive to the relative magnitude of the k_Fq/m and ω_0. The susceptibility $\chi_0(q,\omega_0)$ is always minus for

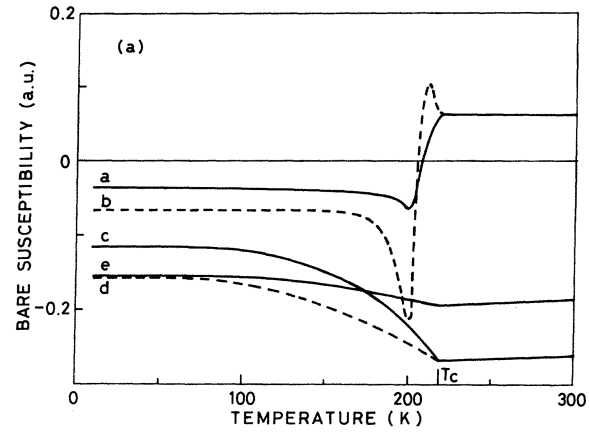

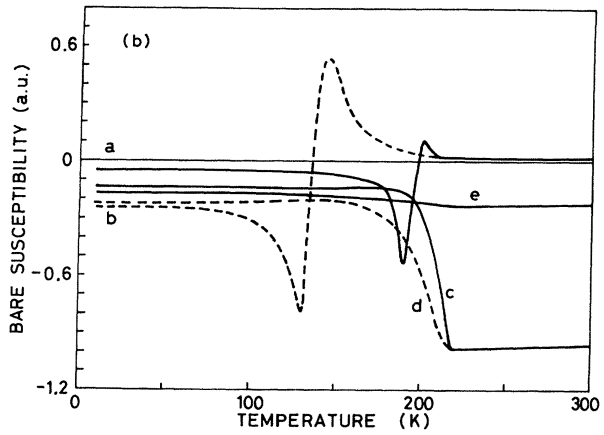

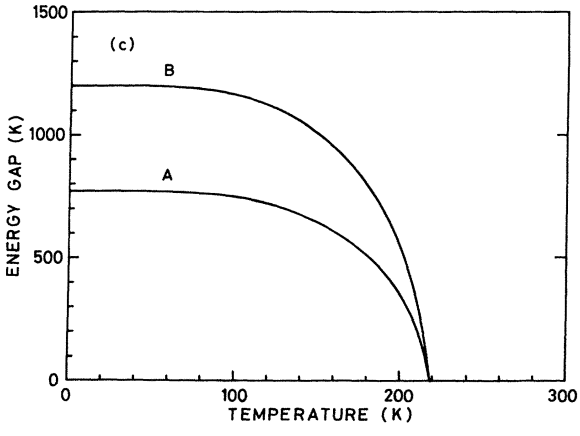

FIG. 14. Temperature dependence of the bare susceptibility (a) χ_0 $(q,\omega_0=284\ cm^{-1})$ and (b) χ_0 $(q,\omega_0=498\ cm^{-1})$ of electron gas in the conduction band which has the CDW gap below the T_c. Solid curves are obtained by assuming the CDW gap to be 1.56 times the superconducting gap [curve B in (c)], and broken curves the same with the superconducting gap [curve A in (c)]. Amount of k_Fq/m is 200 K for curves a and b, 800 K for curves c and d, and 1500 K for curve e.

$k_F q/m > \omega_0$, but $\chi_0(q,\omega_0)$ changes the sign at about the temperature of $E_q \simeq \omega_0$ for $k_F q/m < \omega_0$. When $k_F q/m$ approaches ω_0, $\chi_0(q,\omega_0)$ is enhanced. The wave vector of the incident light spreads inside the metallic material due to the large imaginary part of the refractive index. The magnitude of the $k_F q/m$ is roughly estimated at 1000 K for the wavelength of the light 5145 Å and the lattice constant $c=3.34$ Å, assuming the refractive index 10, the effective electron mass one and the location of the Fermi surface at the middle between the zone center and the edge.

Figure 15 shows the temperature dependence of the integrated scattering intensity of the highest-energy peaks in the 284- and 498-cm^{-1} groups, which are dominant at room temperature. Figures 15(a) and 15(c) show the scattering intensity in the $a(b,b)\bar{a}$ configuration and Figs. 15(b) and 15(d) in the $a(c,c)\bar{a}$ configuration. The scattering intensity in the $a(b,b)\bar{a}$ configuration starts to increase at lower temperature than in the $a(c,c)\bar{a}$ configuration, and suddenly decreases at about 200 K. If the $k_F q/m$ is smaller than the phonon energy, the sudden decrease in the scattering intensity due to the intraband process is observed. The refractive index for the polarization parallel to the b axis is supposed to be smaller than for the polarization parallel to the c axis. The other possibility of the sudden decrease in the scattering intensity in the $a(b,b)\bar{a}$ configuration is due to the change in the refractive index for the light polarized parallel to the b axis, caused by the interchain phase correlation below T_c.

The solid curves in Fig. 15 are calculated from the intraband term M_{intra} and the interband term M_{inter},

$$\frac{d^2\sigma}{d\omega\, d\Omega} = \alpha \,|\, M_{\text{intra}} + M_{\text{inter}} \,|^2 , \tag{3}$$

where M_{intra} is proportional to $\chi_0(q,\omega_0)$ and depends on temperature and M_{inter} is tentatively assumed to be constant with temperature. The three-dimensional character deviated from the perfect one dimensionality gives the k_x and k_y dependence of the electron energy. The distribution of the gap energy due to the dispersion on the x-y plane is assumed by the Gaussian type with the standard deviation 10 K. The average of the energy gap is assumed to be 1.4 times the superconducting gap. If we assume the superconducting gap energy, the jump in the scattering intensity in the $a(b,b)\bar{a}$ configuration appears at about

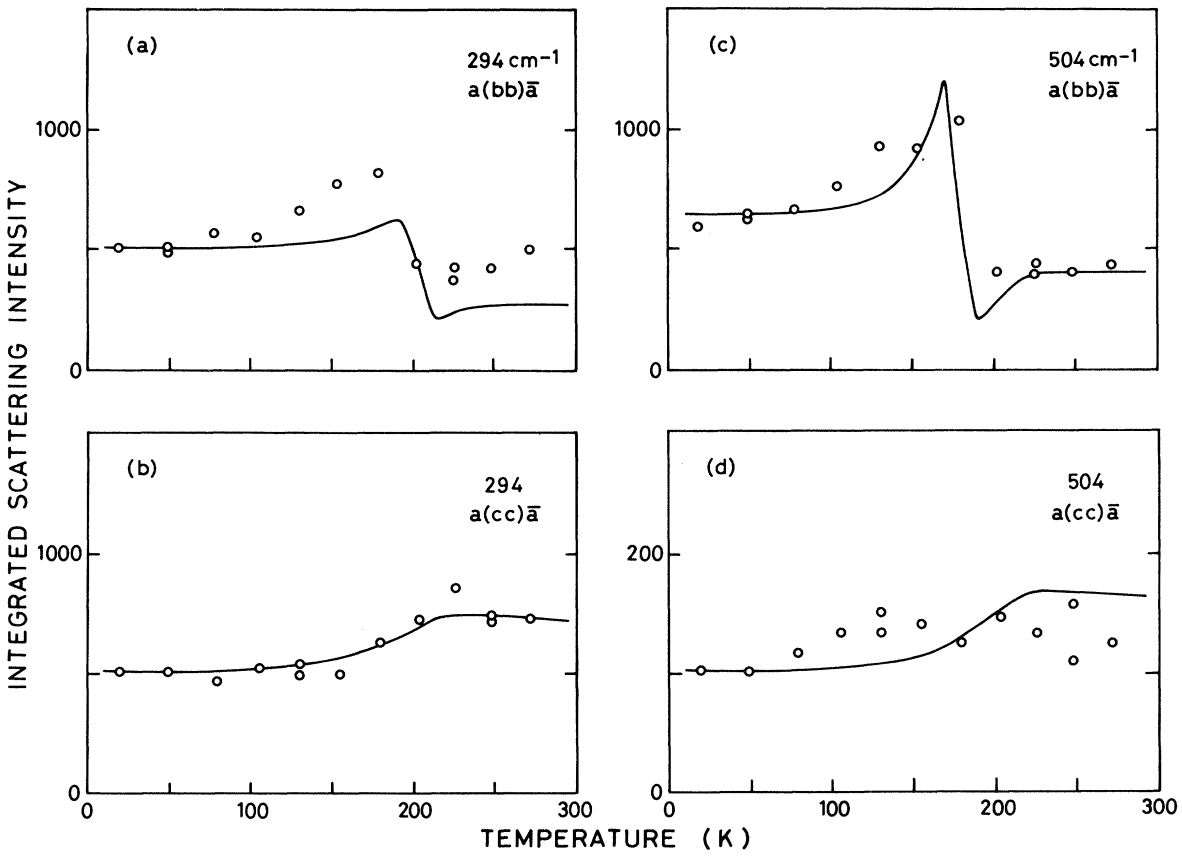

FIG. 15. Temperature dependence of the integrated scattering intensity of the highest-energy peaks in the 284 and 498-cm^{-1} groups in the $a(b,b)\bar{a}$ and $a(c,c)\bar{a}$ polarization configurations. Curves in (a)—(d) are the calculated scattering intensity from the intraband term, which is proportional to the bare susceptibility and the interband term. Parameters in the calculation are written in the text.

150 K. The used parameters are $k_F q/m = 200$ K for the $a(b,b)\bar{a}$ configuration and 1000 K for the $a(c,c)\bar{a}$ configuration, $M_{\text{inter}} = -0.2$ and $\alpha = 8600$ for the 294-cm^{-1} peak in the $a(b,b)\bar{a}$ polarization configuration, $M_{\text{inter}} = -0.2$ and $\alpha = 4400$ for 294 cm^{-1} in $a(c,c)\bar{a}$, $M_{\text{inter}} = -0.25$ and $\alpha = 6500$ for 504 cm^{-1} in $a(b,b)\bar{a}$, and $M_{\text{inter}} = -0.5$ and $\alpha = 230$ for 504 cm^{-1} in $a(c,c)\bar{a}$, where the magnitude of the parameters M_{intra}, M_{inter}, and α are relative. The deviation of the calculated curve from the experimental data is supposed to come from the temperature dependence of the interband term and the complicated three-dimensional character of the CDW gap.

In one-dimensional materials the thermodynamic fluctuation has a large influence on the physical properties. The diffuse line of $0.25c^*$ is observed in x-ray diffraction above T_c,[3] and the effect of fluctuation is also observed in the electric conductivity as a deviation from the metallic temperature dependence between the T_c and room temperature.[3,16] The average energy gap is larger than the gap in the mean-field approximation near T_c due to the fluctuation and the local energy gap remains finite even above the T_c.[33] It brings the deviation in the scattering intensity from the calculation in the mean-field approximation using the CDW gap given by Eq. (2). At this stage it is difficult to estimate the temperature dependence of the fluctuation and the influence to the CDW gap from the Raman scattering spectra because the estimations of the $k_F q/m$ and the interband term are not unique.

The decrease in the scattering intensity due to the destruction of the Fermi surface in the one-dimensional CDW phase transition is in contrast with the two-dimensional case. In $2H$-$TaSe_2$ the intensity of the 240-cm^{-1} A_{1g} phonon peak which is active in the normal phase continues to increase toward 0 K beyond the T_c.[27] The difference comes from the sign between the intraband and the interband terms, and how much of the Fermi surface is destroyed. In one-dimensional materials the Fermi surfaces of the chains related to the phase transition are supposed to be destroyed almost completely below the T_c, while many parts of areas of the Fermi surfaces remain until 0 K in two-dimensional materials.

This polarized high-resolution Raman scattering experiment shows different results from Tsang *et al.*[10] about the phonon linewidth. They related the anomaly of their observed linewidth to the electronic excitation through the CDW gap, but this experiment did not show such an anomaly. It is known that interactions of a phonon with the electronic system cause the large phonon linewidth. A decrease in the lifetime of an acoustic phonon with a large k vector in superconducting Nb_3Sn has been reported by Axe and Shirane.[34] An increase in the optical-phonon linewidth in V_3Si at low temperatures is also explained by the electron-phonon interaction.[35] Sooryakumer and Klein observed an enhancement of the Raman scattering efficiency of the soft CDW mode at the superconducting gap energy in $2H$-$NbSe_2$.[36,37] It was explained by the interaction of the phonon with the electronic excitation through the superconducting gap. In the case of TaS_3 our observed increase of the phonon linewidths toward T_c is explained by the thermodynamic fluctuation near T_c.

In conclusion, the decrease of the scattering intensities of the higher-energy main peaks is attributed to the decrease of the Raman cross section of the intraband process due to the formation of the CDW gap at the Fermi energy. The large change in the low-wave-vector susceptibility χ $(q \simeq 0, \omega_0)$ in TaS_3 below T_c suggests the almost complete destruction of the Fermi surface compared with layered transition-metal dichalcogenides.

ACKNOWLEDGMENTS

The author would like to thank K. Yakushiji for his assistance and T. Sambongi and J. Nakahara for providing the TaS_3 crystals. The author also thanks S. Tanda and T. Taguchi for the x-ray analysis of the crystal.

APPENDIX

Two mechanisms contribute to the Raman scattering probability in metal.[3,4] One is the intraband transition process coming from the electron-radiation interaction of the A^2 term as shown in Fig. 16(a). In this process an electron-hole pair is created in the partially filled conduction band. Sometimes this process is called the diamagnetic process. In this process only the totally symmetric phonon mode is active so that the $\langle k \mid V \mid k \rangle$ is nonvanishing, where $\mid k \rangle$ is the wave function of the conduction electron, V is the deviation of the electronic potential due to the normal coordinate of the phonon. This term exists only in metal. Another mechanism is the interband process as shown in Fig. 16(b). This process is called the paramagnetic process. An electron is excited to the conduction band from the valence band by the $\vec{P}\cdot\vec{A}$ term. In insulating materials only this process contributes to the Raman scattering probability. This mechanism was investigated by Loudon.[28]

The intraband process is very strongly influenced by the density of states of the conduction band at the Fermi energy. The differential cross section for the intraband term is given by[25]

$$\left.\frac{d^2\sigma}{d\omega\, d\Omega}\right|_{\text{intra}} = r_0^2(\hat{e}_i\cdot\hat{e}_s)^2(n+1)[V\chi_0(q,\omega_0)]^2 ,$$

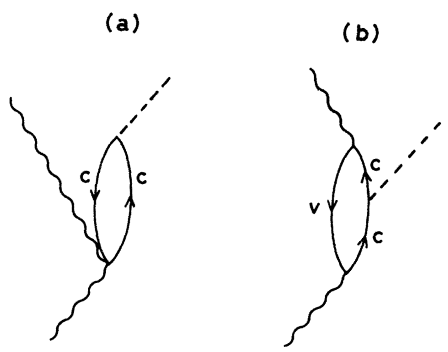

FIG. 16. Raman scattering process of the (a) intraband and the (b) interband terms.

where

$$r_0=\frac{e^2}{mc^2},\quad V=\frac{G\Xi}{\sqrt{2MN\omega_0}},$$

and

$$\chi_0(q,\omega_0)=\sum_k \frac{f(\epsilon^c_{k-q})-f(\epsilon^c_k)}{\epsilon^c_{k-q}-\epsilon^c_k-\omega_0-i\delta}.$$

Here e and m are the electron charge and mass, respectively. $\hat{e}_i$ and $\hat{e}_s$ are the polarization vectors for the incident and scattered photons, n is the Bose-Einstein distribution function for the phonon, G is the absolute value of the reciprocal-lattice vector, Ξ is the deformation potential, and M, N, and ω_0 are the ionic mass, the total number of atoms, and the phonon frequency, respectively. The function f is the Fermi-Dirac distribution function. The dielectric constant $\epsilon(q,\omega_0)$ is given by $1-\varphi\chi_0(q,\omega_0)$, where $\varphi=4\pi e^2/q^2\epsilon_\infty$ is the Fourier transform of the Coulomb interaction. The susceptibility $\chi_0(q,\omega_0)$ is approximated at low temperatures for the gradual density of states at the Fermi energy by

$$\chi_0(q,\omega_0)\propto\rho(E_F),$$

for $\omega_0 \ll \epsilon_{k_F}-\epsilon_{k_F-q}$. In the case of the formation of the energy gap E_g at the Fermi energy, $\chi_0(q,\omega_0)$ is approximated as

$$\chi_0(q,\omega_0)\propto q/E_g$$

for small q and ω_0 and $kT \ll E_g$. The contribution to the scattering intensity from the intraband process decreases with the formation of the CDW gap.

[1]J. A. Wilson, Phys. Rev. B 19, 6456 (1979).
[2]F. Hulliger, in *Structural Chemistry of Layer-Type Phases,* edited by F. Lévy (Reidel, Boston, 1976), p. 247.
[3]T. Sambongi, K. Tsutsumi, Y. Shiozaki, M. Yamamoto, K. Yamaya, and Y. Abe, Solid State Commun. 22, 729 (1977).
[4]K. Tsutsumi, T. Takagaki, M. Yamamoto, Y. Shiozaki, M. Ido, T. Sambongi, K. Yamaya, and Y. Abe, Phys. Rev. Lett. 39, 1675 (1977).
[5]T. Sambongi, M. Yamamoto, K. Tsutsumi, Y. Shiozaki, K. Yamaya, and Y. Abe, J. Phys. Soc. Jpn. 42, 1421 (1977).
[6]P. Monceau, J. Peyrard, J. Richard, and P. Molinié, Phys. Rev. Lett. 39, 161 (1977).
[7]E. Bjerkelund and A. Kjekshus, Z. Anorg. Allg. Chem. 328, 235 (1964).
[8]G. van Tendeloo, J. van Landuyt, and S. Amelinckx, Phys. Status Solidi A 43, K137 (1977).
[9]K. Tsutsumi, T. Sambongi, S. Kagoshima, and T. Ishiguro, J. Phys. Soc. Jpn. 44, 1735 (1978).
[10]J. C. Tsang, C. Hermann, and M. W. Shafer, Phys. Rev. Lett. 40, 1528 (1978).
[11]M. Ido, K. Tsutsumi, T. Sambongi, and N. Môri, Solid State Commun. 29, 399 (1979).
[12]T. Takoshima, M. Ido, K. Tsutsumi, T. Sambongi, S. Honma, K. Yamaya, and Y. Abe, Solid State Commun. 35, 911 (1980).
[13]A. H. Thompson, A. Zettl, and G. Grüner, Phys. Rev. Lett. 47, 64 (1981).
[14]C. M. Jackson, A. Zettl, and G. Grüner, Solid State Commun. 39, 531 (1981).
[15]A. Zettl and G. Grüner, Phys. Rev. B 25, 2081 (1982).
[16]A. Zettl, G. Grüner, and A. H. Thompson, Phys. Rev. B 26, 5760 (1982).
[17]A. Zettl, C. M. Jackson, and G. Grüner, Phys. Rev. B 26, 5773 (1982).
[18]G. Grüner, A. Zettl, W. G. Clark, and A. H. Thompson, Phys. Rev. B 23, 6813 (1981).
[19]R. M. Fleming and C. C. Grimes, Phys. Rev. Lett. 42, 1423 (1979).
[20]E. Bjerkelund, J. H. Fermor, and A. Kjekshus, Acta Chem. Scand. 20, 1836 (1966).
[21]A. Meerschaut, L. Guemas, and J. Rouxel, J. Solid State Chem. 36, 118 (1981).
[22]M. Tanaka and R. Saito (private communication).
[23]N. Shima, J. Phys. Soc. Jpn. 51, 11 (1982).
[24]N. Shima, J. Phys. Soc. Jpn. 52, 578 (1983).
[25]P. M. Platzman and N. Tzoar, Phys. Rev. 182, 510 (1969).
[26]D. L. Mills, A. A. Maradudin, and E. Burstein, Ann. Phys. (N.Y.) 56, 504 (1970).
[27]S. Sugai and K. Murase, Phys. Rev. B 25, 2418 (1982).
[28]R. Loudon, Adv. Phys. 13, 423 (1964).
[29]M. Ido, K. Kawabata, T. Sambongi, K. Yamaya, and Y. Abe, Mol. Cryst. Liq. Cryst. 81, 91 (1982).
[30]D. W. Scott, J. P. McCullough, and H. F. Kruse, J. Mol. Spectrosc. 13, 313 (1964).
[31]S. Sugai, K. Murase, S. Uchida, and S. Tanaka, Solid State Commun. 40, 399 (1981).
[32]M. V. Klein, Phys. Rev. B 24, 4208 (1981).
[33]W. L. McMillan, Phys. Rev. B 16, 643 (1977).
[34]J. D. Axe and G. Shirane, Phys. Rev. Lett. 30, 214 (1973).
[35]H. Wipf, M. V. Klein, B. S. Chandrasekhar, T. H. Geballe, and J. H. Wernick, Phys. Rev. Lett. 41, 1752 (1978).
[36]R. Sooryakumar and M. V. Klein, Phys. Rev. B 23, 3213 (1981).
[37]R. Sooryakumar, M. V. Klein, and R. F. Frindt, Phys. Rev. B 23, 3222 (1981).